

SISTEME CURCUMINĂ - HIDROXIAPATITĂ PENTRU TRATAMENTUL CANCERULUI OSOS CURCUMIN - HYDROXYAPATITE SYSTEMS USED FOR BONE CANCER TREATMENT

IONELA ANDREEA NEACȘU^{1,2}, LILIA MATEI³, ALEXANDRA CĂTĂLINA BÎRCĂ¹, ADRIAN IONUȚ
NICOARĂ^{1,2}, VLADIMIR LUCIAN ENE^{1,2*}, LAURA DENISA DRAGU³, ANTON FICAI^{1,2}, CORALIA BLEOTU³,
ECATERINA ANDRONESCU^{1,2}

¹Department of Science and Engineering of Oxide Materials and Nanomaterials, Faculty of Applied Chemistry and Materials Science, University Politehnica of Bucharest, No. 1-7, Gh. Polizu street, Postal Code 011061, Bucharest, Romania

²Academy of Romanian Scientists, 54 Independentei, 050094, Bucharest, Romania

³Cellular and Molecular Pathology Department, Stefan S. Nicolau Institute of Virology, 285 Mihai Bravu Avenue, 030304, Romania

The purpose of this study was to obtain and characterize curcumin-loaded hydroxyapatite materials for bone cancer treatment. The hydroxyapatite synthesis was performed under controlled conditions in order to obtain monodisperse, fine nanoparticles and to avoid later uncontrolled deposition of these nanoparticles, starting from Ca(OH)₂ and (NH₄)₂HPO₄. The obtained dried precipitate was thermal treated, then suspended in curcumin – dichloromethane solution (where curcumin was added in order to represent 5%, 10% wt. from the amount of hydroxyapatite) and homogenized until solvent evaporation. Morphological and structural characterization, as well as in vitro characterization were performed. All samples were biologically tested and antitumor studies were performed.

Scopul acestui studiu a constat în sinteza și caracterizarea unor materiale pe bază de hidroxiapatită încărcată cu curcumină pentru tratamentul cancerului osos. Sinteza hidroxiapatitei a fost efectuată pornind de la Ca(OH)₂ și (NH₄)₂HPO₄, în condiții controlate, pentru a obține nanoparticule fine monodisperse și pentru a evita aglomerarea ulterioară necontrolată a acestora. Precipitatul obținut a fost uscat, calcinat, apoi suspendat în soluție de curcumină – diclormetan (în care curcumina adăugată a reprezentat 5%, 10% masic din cantitatea de hidroxiapatită) și omogenizat până la evaporarea solventului. Sistemele obținute au fost caracterizate din punct de vedere morfologic și structural, precum și din punct de vedere al comportamentului in vitro. Toate probele au fost de asemenea testate biologic, efectuându-se studii antitumorale.

Keywords: bone cancer treatment, curcumin, hydroxyapatite

1. Introduction

When it comes to cancer-affected tissues, bone tissue is unique through its activity, in the sense that it presents an important characteristic, namely constant remodeling. This occurs due to sequential osteoclastic resorption and osteoblastic bone formation. The remodeling phenomenon is dependent on growth factors and circulating systemic hormones, and at the same time is highly coordinated under normal conditions to support a balance between bone resorption and new bone formation [1], [2]. The occurrence of cancer persists to increase. Bone metastases are considered to be a common cause of many types of malignant cancers [3]. They may occur as skeletal-related events such as spinal cord compression [4], pathological fracture [5], or hypercalcemia [6] and ultimately lead to excruciating bone pain.

Currently, the most used treatment options for bone cancer are chemotherapy, radiotherapy, and surgery. In most cases, patients should have a combination of these three treatment methods for later observation of the effects [7][8]. For the first method of treatment different chemotherapeutic agents are used, such as cisplatin [9], paclitaxel [10],

doxorubicin [11], bisphosphonates [12]. In the case of tumor-induced hypercalcemia, bisphosphonates are considered the standard treatment because they prevent the development of bone metastases. The mode of action of these bisphosphonates is represented by their binding to bone matrix hydroxyapatite crystals, achieving very high local concentrations in the resorption cavity where they are incorporated by the osteoclasts, hence causing apoptosis [13]. Several substances having a similar effect to bisphosphonates activity have been studied for this purpose, and recent studies have shown that the antiresorptive effects of curcumin on bone remodeling works the same way [14]. A study by French *et al.* consisting in the evaluation of long-term activity of curcumin administered as treatment in adult rats suffering from ovariectomy concluded that curcumin performed favorable changes in bone movement and an improvement in bone strength in the ovariectomized adult rat model of postmenopausal osteoporosis [15].

At this point, it is recommended to use natural materials for their applications in the biomedical field, in the treatment of certain diseases, especially cancer [16][17][18]. Therefore, this study investigates the activity of curcumin in a hydroxyapatite matrix for bone

* Autor corespondent/Corresponding author,
E-mail: vladimir.l.ene@gmail.com

cancer treatment, based on the already well-studied hydroxyapatite as bone tissue regeneration material. Curcumin has various anti-neoplastic, antimicrobial, and anti-inflammatory properties, which make it suitable for use in treating cancer or arthritis [19][20][21]. Because curcumin can increase cell sensitivity to the drug without harming healthy cells, it has been introduced into several clinical and preclinical studies, demonstrating beneficial effects against several types of cancer [22] [23][24].

2. Materials and Methods

Sodium phosphate dibasic (Na_2HPO_4 , purity $\geq 99.0\%$), calcium hydroxide ($\text{Ca}(\text{OH})_2$, purity 99.995%), ammonium hydroxide solution 28% (NH_4OH , purity $\geq 99.99\%$), dichloromethane (CH_2Cl_2 , purity $\geq 99.9\%$) and curcumin with $\geq 94\%$ curcuminoid content were purchased from Sigma-Aldrich (Darmstadt, Germany). All chemicals were of analytical purity and used with no further purification. The solutions were prepared with ultrapure water.

For the biological evaluation was used the MG-63 cell line (ECACC 86051601), maintained in Dulbecco's Modified Eagle Medium F-12 (DMEM: F12) supplemented with 10% fetal bovine serum (FBS), at 37°C , $5\% \text{CO}_2$, in a humid atmosphere.

2.1. Synthesis of pristine hydroxyapatite

Hydroxyapatite was synthesized by the coprecipitation method, starting from calcium hydroxide $\text{Ca}(\text{OH})_2$ and dibasic ammonium phosphate $(\text{NH}_4)_2\text{HPO}_4$, maintaining the specific Ca/P ratio of 1.67. In the first step, appropriate amounts of Ca^{2+} and PO_4^{3-} precursors were individually dispersed in ultrapure water under continuous magnetic stirring for 1 hour at 500 rpm. Afterward, the $(\text{NH}_4)_2\text{HPO}_4$ solution was added dropwise over the $\text{Ca}(\text{OH})_2$ suspension in order to obtain the desired precipitate. The pH value was maintained at 10.5 with the aid of 28% ammonia solution, under magnetic stirring at 500 rpm for another 2 hours. After 24 hours of maturation (to finish all chemical processes), the obtained precipitate was filtered and washed with ultrapure water until neutral pH. Finally, the samples were subjected to a heat treatment at 80°C for 12 hours for drying, then calcined at 600°C / 3h.

2.2. Synthesis of curcumin loaded hydroxyapatite

Three samples were obtained in order to examine the different effects between them as follows: hydroxyapatite, hydroxyapatite + 5% curcumin (% wt.), and hydroxyapatite + 10% curcumin (% wt.). Specifically, 0.1 g of the synthesized hydroxyapatite powder was dispersed into 5 mL dichloromethane - curcumin solution (where curcumin was added to represent 5% and 10% wt. from the amount of hydroxyapatite, meaning 5 mg , respectively 10 mg) and vigorously

homogenized in a mortar and pestle until solvent evaporation. After evaporation, it was assumed that the entire curcumin quantity is maintained in the final powders. As a reference, non-loaded hydroxyapatite (HAp) was also further analyzed, along with the 2 obtained curcumin-loaded hydroxyapatite samples (HAp+ 5% curcumin and HAp + 10% curcumin).

For later characterization of the samples from a physical point of view, they were dried in vacuum at room temperature for 12 hours, then subjected to X-ray diffraction analysis (XRD), Fourier transformed infra-red analysis (FT-IR,) dynamic light scattering (DLS), UV-Vis spectrometry and scanning electron microscopy (SEM). Because the use of these materials in the medical field is desirable, being in direct contact with the body, their biocompatibility and antitumor activity were also evaluated.

2.3. Morphological and Structural Characterization

X-ray diffraction analysis was performed using a PANalytical Empyrean (from Malvern PANalytical, Bruno, Nederland) in Bragg-Brentano geometry, equipped with an X-ray tube with Cu anode, with in-line focusing, programmable divergent slit on the incident side, and anti-scatter slit. Spectra were collected in the $10\text{-}80^\circ 2\theta$ angle range, with an acquisition step of 0.02° and acquisition time of 100 s per step. SEM investigations were carried out on a Quanta Inspect F50 (Thermo Fisher - former FEI, Eindhoven, Nederland), equipped with a field emission gun (FEG) with 1.2 nm resolution and EDS spectrometer and with 133 eV resolution at $\text{MnK}\alpha$. The microscope was operated at 30 KeV . The investigation of the synthesized powders using the FT-IR method consisted in analyzing a small amount of sample utilizing the Nicolet iS50R model spectrometer. Measurements were performed at room temperature using the Total Reflection Attenuation Module (ATR), with 32 sample scans between 4000 and 400 cm^{-1} at a resolution of 4 cm^{-1} . Spectral data recording was possible by connecting the spectrometer to the data acquisition and processing unit through the Omnic work program. Dynamic Light Scattering (DLS) measurements were performed using a DelsaMax Pro (Beckman Coulter, Indiana, USA) device equipped with a 532 nm laser. The powder was dispersed in ultrapure water, at room temperature and ultrasound for 10 minutes.

Curcumin-loaded hydroxyapatite powders (20 mg) were suspended in simulated body fluid (SBF, 10 mL) and incubated at 37°C . After fixed time intervals varying from 5 min to 36 hours , each suspension was filtered and the filtrate was spectrophotometrically measured at 424 nm , which is the $\lambda \text{ max}$ wavelength for curcumin dissolved in SBF. Based on the standard absorption against the concentration curve, curcumin concentration was

determined, and hence the amount of curcumin released at each time point. The percentage of release at each time point was calculated based on the curcumin amount loaded per mg of material after the loading studies. UV-Vis measurements were made using a ThermoEvolution 300 spectrometer operated in transmission mode over the range of 190-1100 nm. All results are represented as mean ± standard error, n = 3.

2.4. Biological evaluation

Cytotoxicity assay

The toxicity of HAp-curcumin compounds was established using CellTiter 96® AQueous One Solution Cell Proliferation Assay (MTS) (Promega). Briefly, 10⁴ MG63 cells were treated with concentration between 20-0.625 μg/mL for curcumin and 400-12.5 μg/mL for HAP + curcumin samples. The evaluation was performed at 24, 48, and 72 h after MTS adding for 3 h, and reading at TriStar photometer at 490 nm. The half-maximal inhibitory concentration (IC₅₀) was calculated as the concentration of drug necessary to inhibit 50% of MG63 cells.

Cell cycle analysis

MG63 cells were seeded at 1x10⁵ cells/cm² in DMEM: F12 containing 10% foetal bovine serum, and 100 μg/mL HAp + 10%curcumin, 100 μg/mL HAp + 5%curcumin, 5 μg/mL curcumin, and 10 μg/mL curcumin, these being the theoretical maximum curcumin quantities loaded into the hydroxyapatite substrate. DNA content and cell cycle distribution were determined using an XML Beckman Coulter cytometer. Briefly, after 48 h of treatment, MG63 cells were collected, fixed in 70% ethanol overnight at -20 °C, washed twice with PBS, and then incubated with 100 μg/mL propidium iodide (PI) for 30 minutes, shielded from light at room temperature before flow cytometric analysis.

Gene expression analysis

Total RNA was extracted with triazole reagent (Invitrogen, USA) according to the protocol of manufacturer from MG63 cells treated with 100 μg/mL, HAp + 10% curcumin and HAp + 5% curcumin, 5 μg/mL or 10 μg/mL curcumin for 24 hours. For each sample, 2 μg of total RNA was reverse-transcribed using High Capacity cDNA Reverse Transcription Kit with RNase inhibitor (Applied Biosystem), and 50 ng cDNA from each sample was used in the real-time PCR reaction. Real-time PCR was performed on StepOnePlus™ Real-Time PCR System (Applied Biosystems) using pre-validated Taqman Gene Expression Assays kits (Applied Biosystems): *caspase 7* (Hs00169152_m1), *caspase 8* (Hs00154256_m1), *caspase 9* (Hs00154261_m1), *BAX* (Hs00180269_m1), *BCL2* (Hs00153350_m1), *MCL1* (Hs00172036_m1), *Cyclin A* (Hs00153138_m1), *Cyclin B* (Hs00259126_m1), *CDK1* (Hs00938777_m1), *CDC20* (Hs00426680_mH), *PRKAA1* (Hs01562308_m1),

PRKAA2 (Hs00178903_m1), *ARRB1* (Hs00244527_m1), and *GAPDH* (as an endogenous control). Results were analyzed with StepOne Software v2.3 (Applied Biosystems) using the ΔC_T method to compare the relative expression levels.

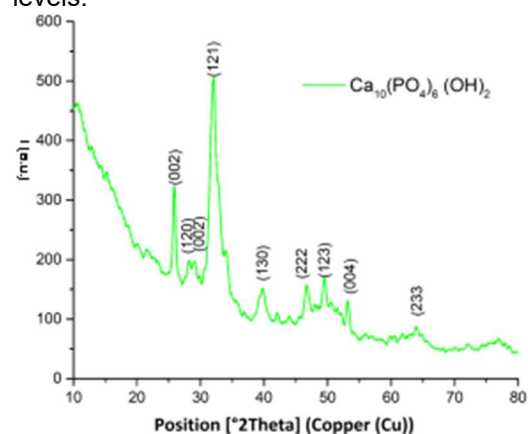


Fig. 1 - XRD pattern for pristine hydroxyapatite / Difractograma de raze X pentru hidroxiapatita neîncărcată.

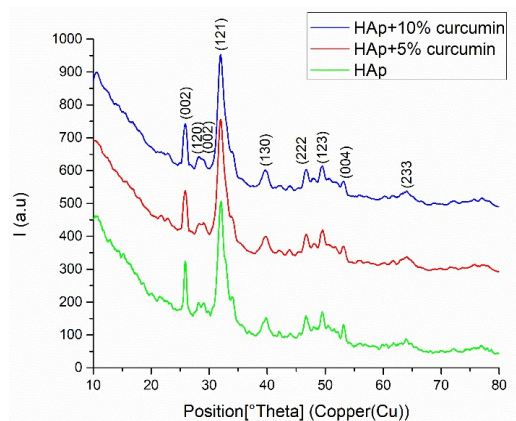


Fig. 2 - XRD patterns for all obtained samples / Difractogramele de raze X pentru toate probele obținute

3. Results and discussion

The qualitative XRD patterns for the calcined pristine hydroxyapatite (Figure 1) and curcumin loaded hydroxyapatite powders (figure 2) highlight the diffraction peaks corresponding to the Miller indices (002), (120), (121), (130), (222), (123), (004), (233), characteristics for hydroxyapatite, according to the data available in the [PDF4 + 00-064-0738] [40] file, as the only crystalline phase. Based on the small intensity registered values and the presence of a diffraction halo at low angles, the crystallinity degree is considered low for HAp but slightly increases with the addition of curcumin.

Scanning Electron Microscopy (SEM) images provide information about the morphology and dimensions of nanoparticles. In the SEM images representative for the unloaded hydroxyapatite, the nanoparticles appear to have needle-like morphology and mostly form agglomerates. In

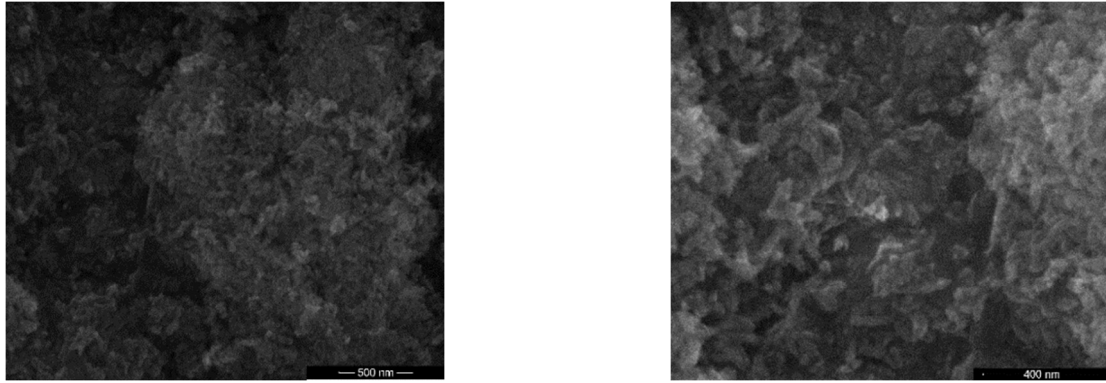


Figure 3 - SEM images for unloaded HAp sample / *Imagini SEM pentru hidroxiapatită neîncărcată*

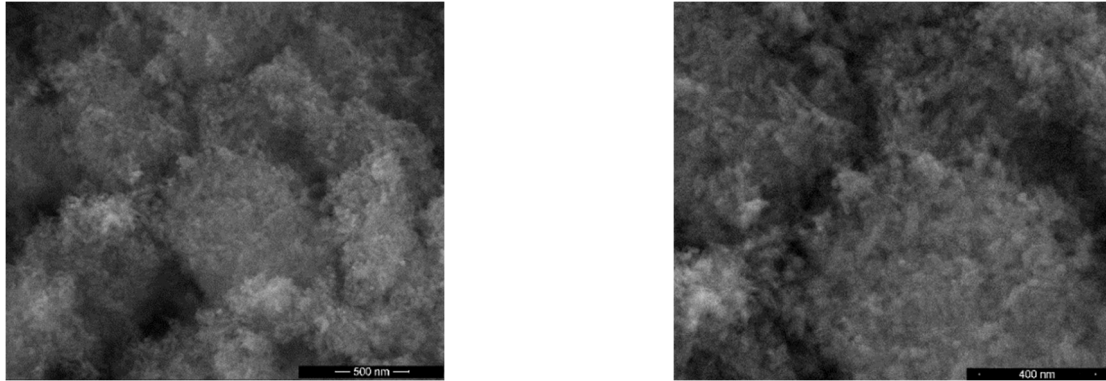


Figure 4 - SEM images for HAp+5%curcumin / *Imagini SEM pentru HAp+5%curcumină*

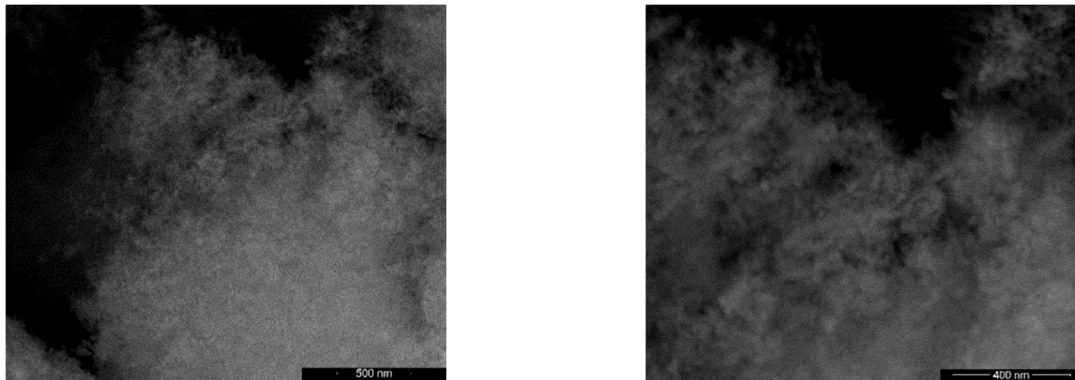


Figure 5 - SEM images for HAp+10%curcumin / *Imagini SEM pentru HAp+10%curcumină*

terms of size, the nanoparticles' width varies between 13-15 nm (Figure 3). The addition of curcumin does not significantly influence the particle's morphology, therefore the needle shape is maintained also for HAp+5%curcumin (Figure 4) and HAp+10%curcumin samples (Figure 5). The dimensions are slightly increasing with the adsorbed curcumin amount, ranging between 12-18 nm for HAp+5%curcumin sample and between 10-25 nm for HAp+10%curcumin sample (for the measurements was used the ImageJ software; for each sample were performed at least 10 measurements on separated, easy to distinguish particles).

The DLS analysis confirms the nanoparticles' tendency to form agglomerates, which in our case have a hydrodynamic diameter of the particle in a water suspension of 4138.5 nm for HAp, 2338.1 nm for HAp+5% curcumin, and 2175.1 nm for HAp+10% curcumin. The dimensions measured by DLS were

higher than the SEM-based measured values, which is understandable, because in DLS large agglomerates mask the presence of small particles and aggregates, giving higher average values. Also, it is known that when the particle size is smaller, there is a higher tendency to form agglomerates due to the higher specific surface area. As can be seen in Figure 6, the particle dimensions have a unimodal distribution, with a polydispersity index (Pdl) of 0 nm for all analyzed samples. Pdl represents the square of the standard deviation divided by the square of the mean for each peak from DLS analysis. Lower Pdl values are characteristic of monodisperse systems, values less than 0.7 indicating greater stability for a nano delivery/colloidal system.

In order to confirm the immobilization of curcumin on hydroxyapatite surface, FT-IR spectra were acquired for all 3 samples and the comparative results are presented in Figure 7 and

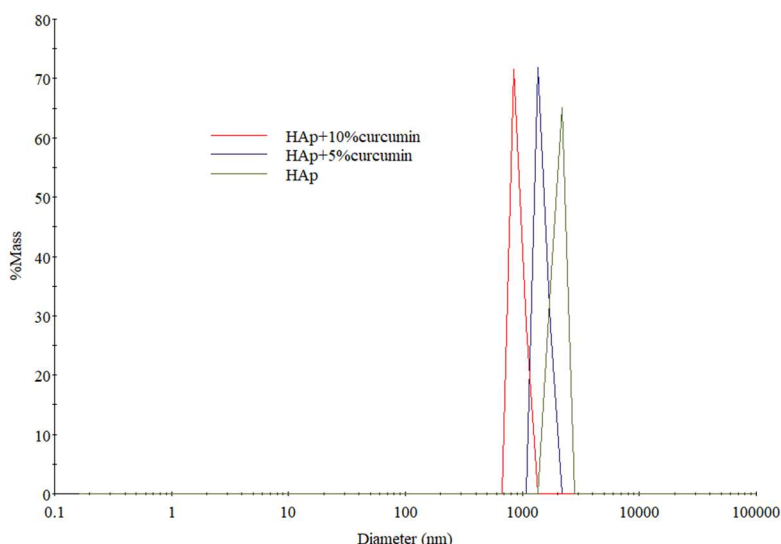


Fig. 6 - DLS analysis of HAp, HAp+5%curcumin and HAp+10%curcumin samples
 Caracteristicile DLS ale probelor HAp, HAp+5%curcumină și HAp+10%curcumină

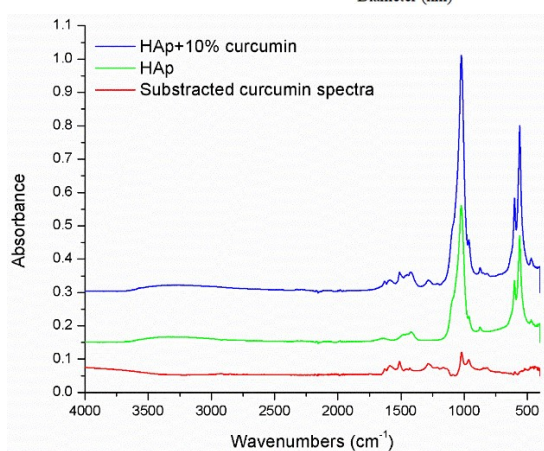


Fig. 7 - FT-IR spectra for HAp and HAp+10%curcumin / Spectre FT-IR pentru HAp și HAp+10%curcumin

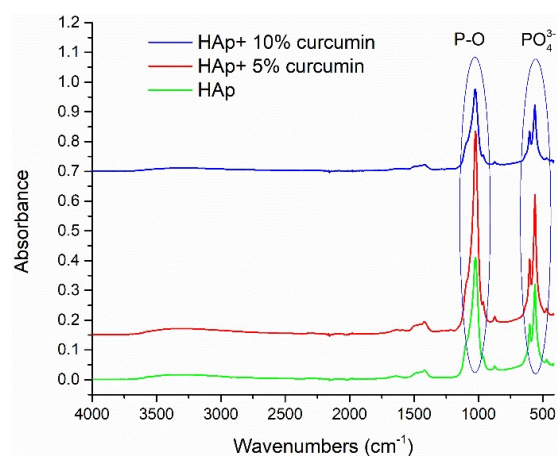


Fig. 8 - FT-IR spectra for all samples / Spectre FT-IR pentru toate probele

Figure 8. When subtracting the unloaded hydroxyapatite spectrum from the HAp+10%curcumin spectrum, the absorption bands corresponding to C = O and C = C at about 1590 cm^{-1} and 1512 cm^{-1} are identified, being specific to curcumin molecule, thus proving the addition onto hydroxyapatite surface. As a consequence, a flattening in the $3200\text{--}3500\text{ cm}^{-1}$ absorption bands is observed, attributed to the extent of the O-H bonds due to the presence of water adsorbed on the hydroxyapatite surface and the phenolic curcumin group. Surface adsorbed water molecules are confirmed also by the presence of water-specific bands observed in the range of $1600\text{--}1650\text{ cm}^{-1}$ occurring in all spectra. The corresponding asymmetric and symmetric P-O absorptions are observed at the wavenumbers between $1000\text{--}1200\text{ cm}^{-1}$, $900\text{--}950\text{ cm}^{-1}$, and $530\text{--}550\text{ cm}^{-1}$, respectively. When comparing the two curcumin-loaded samples, lower intensities of the hydroxyapatite specific bands are observed in the sample with higher curcumin content, because a larger amount of drug shields the vibration of PO_4^{3-} (between 500 cm^{-1} – 600 cm^{-1}) linkages.

Curcumin release from hydroxyapatite was studied in SBF solution with a pH of 7.25, containing

the ionic species and concentrations corresponding to human blood plasma. Due to its hydrophobic properties, curcumin showed limited release from the hydroxyapatite matrix [25]. The results are presented as a percentage from the UV-VIS absorption of pure curcumin in SBF, which represents in this case the 100% release rate. As can be seen, after 36 hours, both curcumin-loaded samples showed only ~20% release of total drug loading, after which the plateau range was achieved. An explanation might emerge from the metal ion chelating ability of curcumin, which determines the curcumin adhesion to the matrix by binding to the calcium ions present in the HAp. For both samples, the drug release presented an initial burst within the first minutes of incubation, followed by a gradual release profile until 24 h (Figure 9).

The cytotoxic effect of nanoparticles loaded with curcumin was evaluated on MG63 cells using MTS assay at 24, 48, and 72 hours (Figure 10). The new complexes' inhibitory effect, as well as the curcumin one, develop in time. After a 72 h treatment with HAp + 5% curcumin, HAp + 10% curcumin and free curcumin, IC_{50} were $17.991\text{ }\mu\text{g/mL}$, $15.483\text{ }\mu\text{g/mL}$, and $5.081\text{ }\mu\text{g/mL}$, respectively (Figure 11A). Still, according to drug

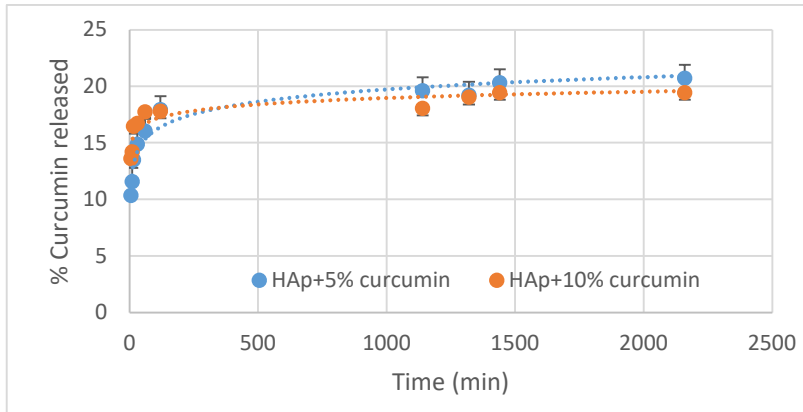


Fig. 9 - Curcumin release profiles from loaded HAp samples / Profilul de eliberare a curcuminei din probele de HAp .

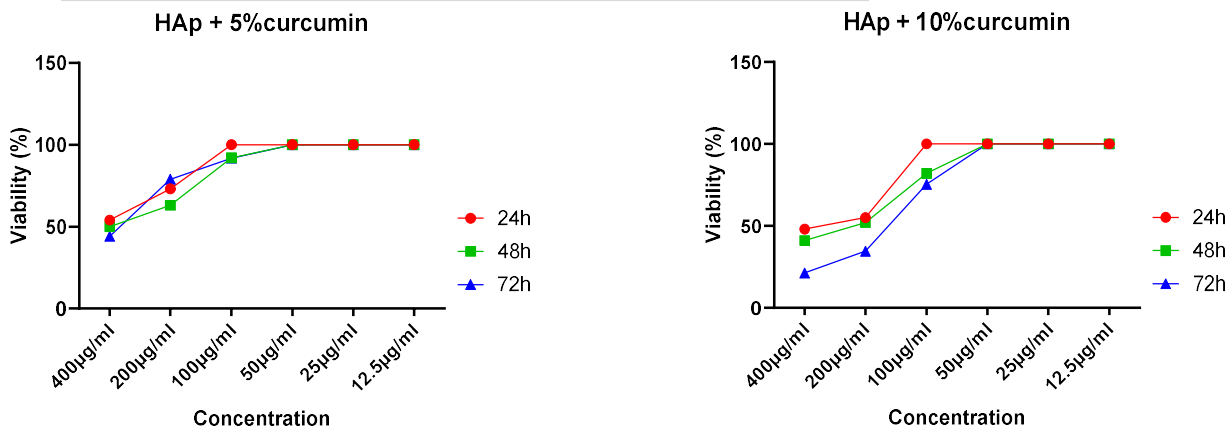


Fig. 10 - The effect of Hap + curcumin on MG-63 cells viability (A) HAp + 5%curcumin (B) HAp + 10%curcumin / Efectul sistemelor curcumina – hidroxiapatita asupra viabilitatii celulelor MG-63 (A) HAp + 5%curcumina (B) HAp + 10%curcumina

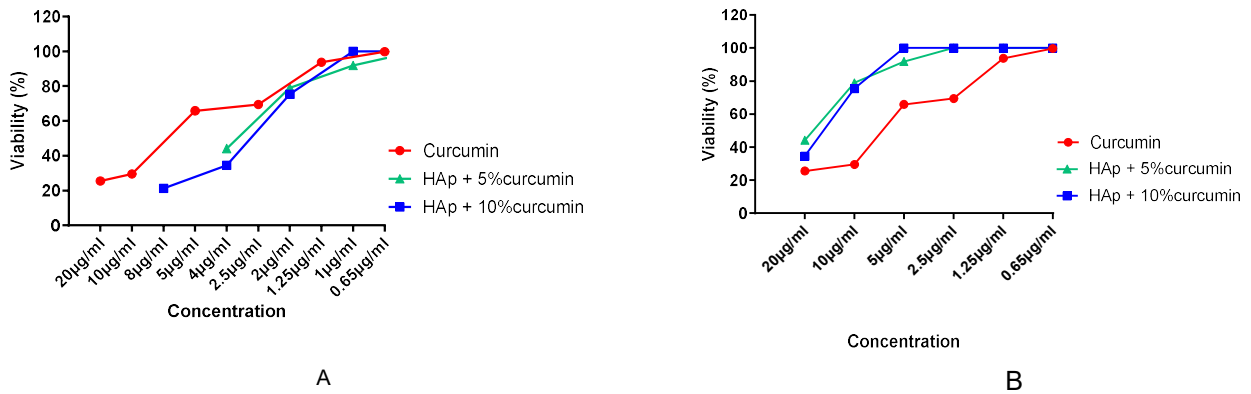


Fig. 11 - MG63 cells viability in function of (A) final concentration of curcumin loaded on hydroxyapatite and of (B) released drug concentration after 72 h treatment / Viabilitatea celulelor MG6 în funcție (A) de concentrația finală de curcumina încărcată în hidroxiapatita și (B) de concentrația curcuminei eliberată după 72h

release studies, after 72 hours, only 20% of curcumin are released by HAp nanoparticles, the released drug concentration that inhibits 50% of MG63 cells being 3.5982 µg/mL for HAp + 5% curcumin and 3.0966 µg/mL for HAp + 10% curcumin (Figure 11B), thus HAp – curcumin complexes proving a better efficiency in time than free curcumin.

At a molecular level, HAp + 5% curcumin tested at 100 µg/mL slightly increased *caspase 9* gene expression indicating the activation of the intrinsic apoptotic pathway, while curcumin, at both tested concentrations, increased *caspase 8* gene expression indicating the activation of extrinsic

apoptotic pathway (Figure 12). Although according to other studies conducted on HT-29 cells curcumin induces apoptosis via the mitochondria-mediated pathway, in the MG-63 cell line, according to our results, curcumin activated the extrinsic pathway. Still, in combination with HAp, curcumin (HAp – 5% curcumin) activated the mitochondria-mediated pathway in MG-63 cells.

The pro-apoptotic *Bax* and anti-apoptotic *Bcl-2* genes expression, *Bax/Bcl-2* ratio was positive for HAp + 10% curcumin and for curcumin (at 5 µg/mL and 10 µg/mL) indicating apoptotic program activation. It was demonstrated that curcumin

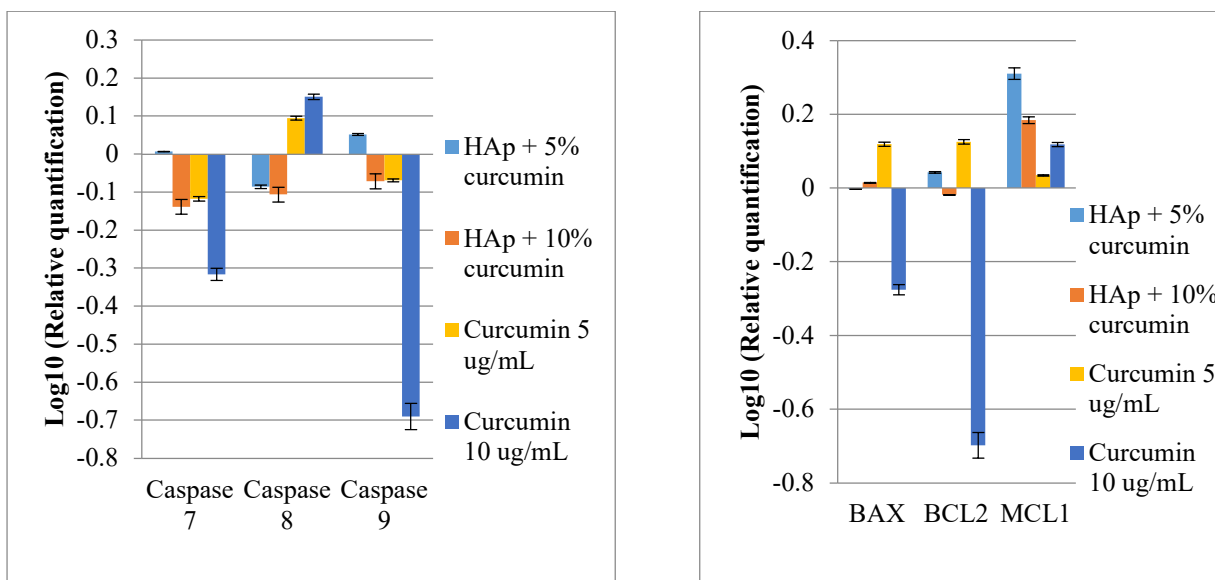


Fig. 12 - The influence of tested compounds on the expression of genes implicated in apoptosis induction in MG-63 cells / *Influența sistemelor curcumină – hidroxiapatită asupra expresiilor genice implicate în inducerea apoptozei celulelor MG-63*

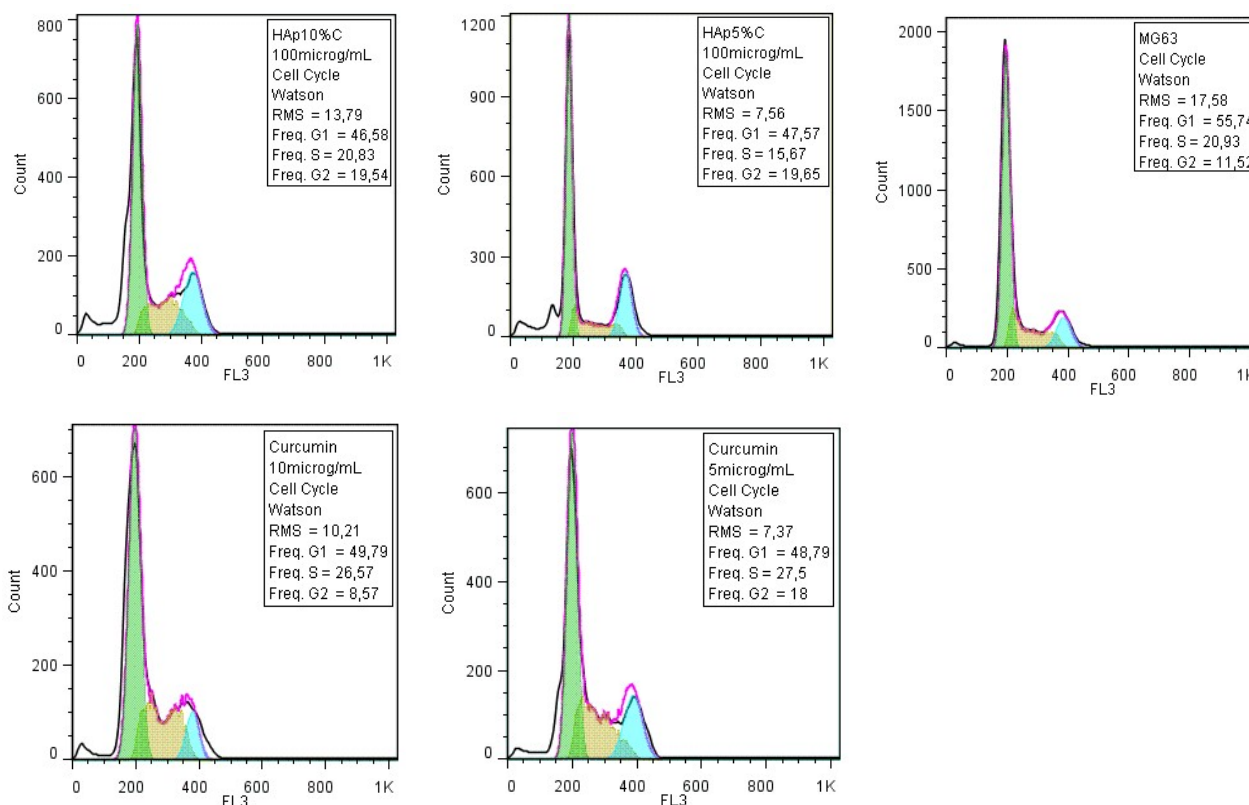


Fig. 13 - Flow cytometer analysis of MG-63 cell cycle after 48 h treatment with tested compounds / *Citometria în flux pentru analiza ciclului celular al MG-63 după 48h de tratament cu sistemele curcumină – hidroxiapatită*

suppressed the expression of the antiapoptotic protein myeloid cell leukemia-1 (*Mcl-1*) 29443732, but in our experiments, at 24 hours, the RNA levels of *Mcl-1* were still increased (Figure 12) being in accordance with cytotoxicity.

Regarding the influence of tested compounds on cell cycle progression, evaluated at 48 hours, it was observed that curcumin increased the G2/M phase, these results being in accordance with literature data that curcumin induces G2/M cell cycle

arrest. Curcumin treatment also decreased G0/G1 phase and increased S phase. HAp + curcumin-induced G2/M phase increase and G0/G1 decrease. Regarding HAp + curcumin influence on S phase, this was decreased by HAp + 5% curcumin and not affected by HAp + 10% curcumin treatment (Figure 13).

At molecular level, curcumin, in a concentration of 10 $\mu\text{g/mL}$, determined the decrease of *Cyclin B*, *CDC20* and *CDK1* genes

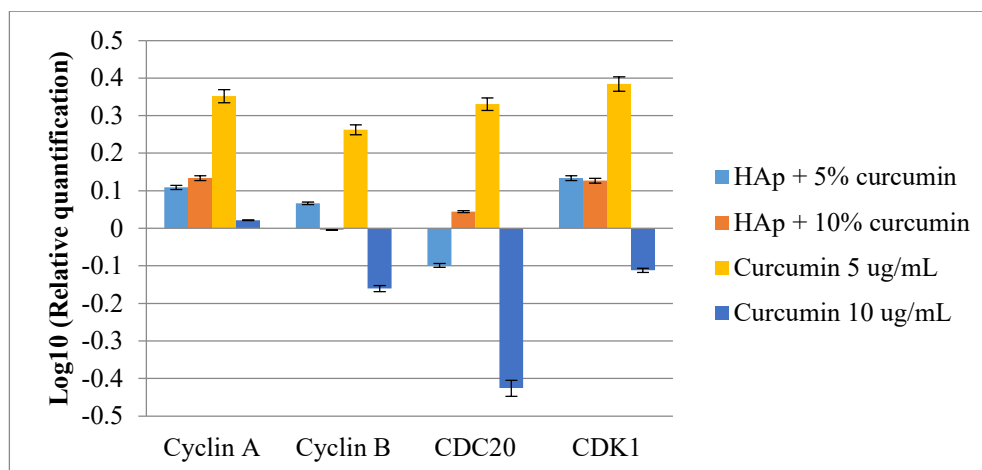


Fig. 14 - The influence of tested compounds on the expression of Cyclin A, Cyclin B, CDK1, and CDC20 genes in MG-63 cells / *Influența sistemelor curcumină – hidroxiapatită asupra expresiilor genice ale ciclinei A, ciclinei B, CDK1 și CDC20 din celulele MG-63*

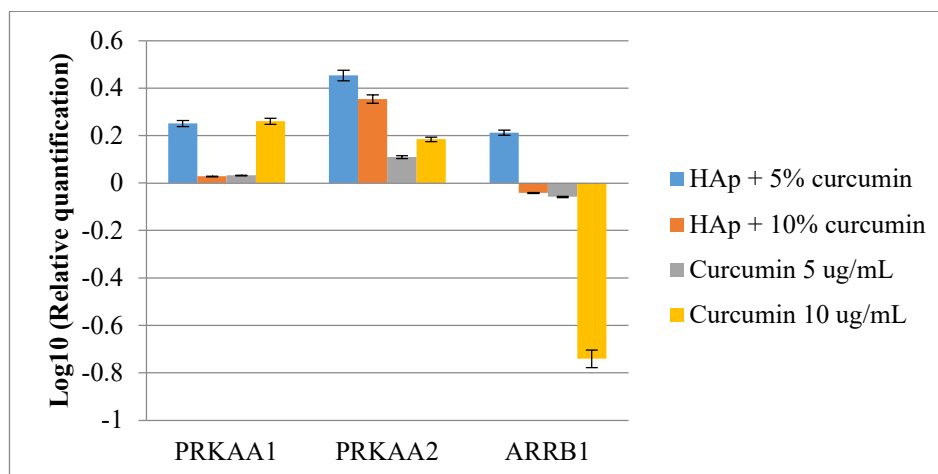


Fig. 15 - The influence of tested compounds on the expression of PRKAA1, PRKAA2, and ARRB1 genes in MG-63 cells / *Influența sistemelor curcumină – hidroxiapatită asupra expresiilor genice ale PRKAA1, PRKAA2 și ARRB1 din celulele MG-63*

expressions after 24 h treatment, indicating a G2/M cell cycle arrest observed also at cell cycle evaluation through flow cytometry. At 5 $\mu\text{g/mL}$, curcumin increased *Cyclin A*, *Cyclin B*, *CDC20*, and *CDK1* genes expressions.

These results correlate with curcumin cytotoxicity evaluated by the MTS method that showed no toxic effects for curcumin at 5 $\mu\text{g/mL}$ after 24 hours. Regarding HAp – curcumins activity, they increased the gene expressions of *Cyclin A* and *CDK1*, the nanoparticles coupled with 5% curcumin increasing also *Cyclin B* and decreasing *CDC20* gene expressions, while those coupled with 10% curcumin increased *CDC20* gene expression (Figure 14).

Also, all tested compounds increased *Protein Kinase AMP-Activated Catalytic Subunit Alpha 1 and 2 (PRKAA1 and PRKAA2)* genes expressions (Figure 15) indicating activation of AMP-activated protein kinase (AMPK) that inhibits the mTOR pathway and blocks cell cycle progression. These

results match with literature data that curcumin activates the AMPK pathway. Also, curcumin, tested at 10 $\mu\text{g/mL}$, induced beta-arrestin 1 (*ARRB1*) decreased expression that was slightly decreased also by curcumin tested at 5 $\mu\text{g/mL}$ and by HAp + 10% curcumin (Figure 14). *ARRB1*, being implied in the mitogen-activated protein kinase (MAPK) signaling pathway, mediates prolonged phosphorylation of ERK1/2 and Akt that are involved in regulating *CDC25C/CDK1/cyclin B1* activity, *ARRB1* knockdown inducing G2/M phase cell cycle arrest.

4.Conclusions

Hydroxyapatite synthesis through the co-precipitation method led to crystalline, monodispersed nanoparticles, with acicular morphology. Following the biological evaluation, it was demonstrated that the hydroxyapatite-curcumin systems have a cytotoxic effect on bone

cancer cells, activating apoptosis, and increasing the level of AMPK, ARRB1 associated with a G2/M cell cycle. Moreover, the obtained systems exhibited biological properties dependent on the concentration and release profile of curcumin from loaded HAp samples. This is a very useful property that can be assessed to reduce the harmful effects on normal bystander cells when using high curcumin concentration per dose. Our results demonstrate that newly developed nanocomposites possess good antitumor properties, but further *in vivo* tests are needed

Acknowledgments

The financial contribution received from the national project: "Innovative biomaterials for treatment and diagnosis" BIONANOINOV, (PN-III/1-1.2-PCCD-I/2017-0629) is highly acknowledged. The SEM, FTIR, and DLS analyses obtained on the samples were possible due to the EU-funding project POSCCE-A2-O2.2.1-2013-1/Priority Axe 2, Project No. 638/12.03.2014, ID 1970, SMIS-CSNR code 48652. The XRD analyses were possible due to the European Social Fund and Romanian Government financing under the contract number POSDRU/86/1.2/S/58146 (MASTERMAT).

REFERENCES

[1] H. C. Blair et al., "Osteoblast differentiation and bone matrix formation in vivo and in vitro," *Tissue Engineering - Part B: Reviews*, 2017, **23** (3), p. 268–280.

[2] U. H. Lerner, E. Kindstedt, and P. Lundberg, "The critical interplay between bone resorbing and bone forming cells," *J. Clin. Periodontol.*, 2019, **46**(S21), p. 33–51.

[3] R. E. Coleman et al., "Bone metastases," *Nature Reviews Disease Primers*, 2020, **6**(1), p. 1–28.

[4] S. Hong, T. Youk, S. J. Lee, K. M. Kim, and C. M. Vajdic, "Bone metastasis and skeletal-related events in patients with solid cancer: A Korean nationwide health insurance database study," *PLoS One*, 2020, **15**(7):e0234927.

[5] L. M. Kelley et al., "Pathological fracture and prognosis of high-grade osteosarcoma of the extremities: An analysis of 2,847 consecutive cooperative Osteosarcoma Study Group (COSS) patients," *J. Clin. Oncol.*, 2020, **38**(8), 823–833.

[6] J. Zagzag, M. I. Hu, S. B. Fisher, and N. D. Perrier, "Hypercalcemia and cancer: Differential diagnosis and treatment," *CA. Cancer J. Clin.*, 2018, **68**(5), 377–386.

[7] H. Chen and Y. Yao, "Progress of biomaterials for bone tumor therapy," *J. Biomater. Appl.*, 2021, p.08853282211035236.

[8] L. Ambrosio, M. G. Raucchi, G. Vadalà, L. Ambrosio, R. Papalia, and V. Denaro, "Innovative biomaterials for the treatment of bone cancer," *International Journal of Molecular Sciences*, 2021, **22**(15), 8214.

[9] E. Andronescu et al., "Collagen-hydroxyapatite/cisplatin drug delivery systems for locoregional treatment of bone cancer," *Technol. Cancer Res. Treat.*, 2013, **12**(4), 275–284.

[10] E. M. Alexandrino et al., "Paclitaxel-loaded polyphosphate nanoparticles: A potential strategy for bone cancer treatment," *J. Mater. Chem. B*, 2014, **2**(10), 1298–1306.

[11] M. S. ur Rahman et al., "Osteogenic silver oxide doped mesoporous bioactive glass for controlled release of doxorubicin against bone cancer cell line (MG-63): In vitro and in vivo cytotoxicity evaluation," *Ceram. Int.*, 2020, **46**(8), 10765–10770.

[12] V. F. Zymperdikas, M. P. Yavropoulou, E. G. Kaklamanos, and M. A. Papadopoulos, "Bisphosphonates as Supplement to Dental Treatment: A Network Meta-Analysis," *Journal of Dental Research*, 2021, **100**(4), 341–351.

[13] T.-S. Fu, T.-S. Huang, C.-C. Sun, Y.-C. Shyu, and F.-P. Chen, "Impact of bisphosphonates and comorbidities on initial hip fracture prognosis," *Bone*, 2021, **154**, 116239.

[14] X. Chen et al., "Curcumin activates DNA repair pathway in bone marrow to improve carboplatin-induced myelosuppression," *Sci. Rep.*, 2017, **7**(1), 1–11.

[15] D. L. French, J. M. Muir, and C. E. Webber, "The ovariectomized, mature rat model of postmenopausal osteoporosis: An assessment of the bone sparing effects of curcumin," *Phytomedicine*, 2008, **15**(12), 1069–1078.

[16] I. I. Lungu, A. M. Grumezescu, A. Volceanov, and E. Andronescu, "Nanobiomaterials used in cancer therapy: An up-to-date overview," *Molecules*, 2019, **24**(19), 3547.

[17] A. Ficăi, C. Marques, J. M. F. Ferreira, E. Andronescu, D. Ficăi, and M. Sonmez, "Multifunctional materials for bone cancer treatment," *Int. J. Nanomedicine*, 2014, **9**(1), 2713-2725.

[18] D. Kashyap et al., "Natural product-based nanoformulations for cancer therapy: Opportunities and challenges," *Seminars in Cancer Biology*, 2021, **69**, 5–23.

[19] P. Basnet and N. Skalko-Basnet, "Curcumin: An anti-inflammatory molecule from a curry spice on the path to cancer treatment," *Molecules*, 2011, **16**(6), 4567–4598.

[20] M. C. Fadus, C. Lau, J. Bikhchandani, and H. T. Lynch, "Curcumin: An age-old anti-inflammatory and anti-neoplastic agent," *Journal of Traditional and Complementary Medicine*, 2017, **7**(3), 339–346.

[21] I. R. Afrida, F. Fatchiyah, N. Widodo, M. Amin, and M. S. Djati, "Shogaol, bisdemethoxycurcumin, and curcuminoid: Potential zingiber compounds against covid-19," *Biointerface Res. Appl. Chem.*, 2021, **11**(5), 12869–12876.

[22] D. D. Abd El-Monem, A. A. S. Abdel Rahman, and S. H. B. Elwakeel, "Nanocurcumin improves the therapeutic role of mesenchymal stem cells in liver fibrosis rats," *Biointerface Res. Appl. Chem.*, 2021, **11**(6), 14463–14479.

[23] Y. Wei, X. Pu, and L. Zhao, "Preclinical studies for the combination of paclitaxel and curcumin in cancer therapy (Review)," *Oncology Reports*, 2017, **37**(6), 3159–3166.

[24] A. Allegra, V. Innao, S. Russo, D. Gerace, A. Alonci, and C. Musolino, "Anticancer Activity of Curcumin and Its Analogues: Preclinical and Clinical Studies," *Cancer Investigation*, 2017, **35**(1), 1–22.

[25] T. Raja Sekharan, R. Margret Chandira, S. C. Rajesh, S. Tamilvanan, C. T. Vijayakumar, and B. S. Venkateswarlu, "Ph, viscosity of hydrophobic based natural deep eutectic solvents and the effect of curcumin solubility in it," *Biointerface Res. Appl. Chem.*, 2021, **11**(6), 14620–14633.
